Drying Technology
An International Journal

ISSN: 0737-3937 (Print) 1532-2300 (Online) Journal homepage: http://www.tandfonline.com/loi/ldrt20

Reduction of a model for single droplet drying and application to CFD of skim milk spray drying

T. T. H. Tran, M. Jaskulski & E. Tsotsas

To cite this article: T. T. H. Tran, M. Jaskulski & E. Tsotsas (2017) Reduction of a model for single droplet drying and application to CFD of skim milk spray drying, Drying Technology, 35:13, 1571-1583, DOI: 10.1080/07373937.2016.1263204

To link to this article: http://dx.doi.org/10.1080/07373937.2016.1263204

Accepted author version posted online: 08 May 2017.
Published online: 08 May 2017.

DRYING TECHNOLOGY
2017, VOL. 35, NO. 13, 1571–1583
https://doi.org/10.1080/07373937.2016.1263204

Taylor & Francis
Taylor & Francis Group

Reduction of a model for single droplet drying and application to CFD of skim milk spray drying

T. T. H. Tran[a], M. Jaskulski[b], and E. Tsotsas[c]

[a]School of Heat Engineering and Refrigeration, Hanoi University of Science and Technology, Hanoi, Vietnam; [b]Faculty of Process and Environmental Engineering, Lodz University of Technology, Lodz, Poland; [c]Thermal Process Engineering, Otto von Guericke University Magdeburg, Magdeburg, Germany

ABSTRACT

In this work, a novel methodology for the development of a high-accuracy computational fluid dynamics (CFD) model for the spray-drying process is described. Starting point is an own spatially resolving model of droplet/particle drying, which was developed and validated on the basis of a series of single droplet drying (SDD) experiments. This sophisticated model is transformed to a much simpler version: the characteristic drying curve approach, after running the full SDD model in a wide range of operating conditions. Then, the obtained reduced model is implemented into the CFD solver. The CFD spray-drying model takes into account the hydrodynamics of the continuous phase, particle drying kinetics, changes in the particle diameter, and the heat loss from the drying chamber to the environment. Validation of the entire procedure is provided by data obtained from drying experiments performed in a co-current laboratory spray tower. High accuracy of the developed CFD model of skim milk spray drying has been found for both phases, for the mean outlet temperature of the continuous phase (air) and for the change in average particle moisture content along the spray tower (discrete phase).

KEYWORDS

CFD; model reduction; single droplet drying; skim milk; spray drying

Introduction

Spray drying is one of the most common methods used in industry for powder production. Though simple to perform, spray drying is very complex in terms of heat, mass and momentum transfer between phases. There are many parameters that have an effect on process and product quality, not only operational conditions like air temperature, feed flow rate, or the way of phase mixing (co-current or counter-current), but also parameters that depend on dryer geometry like hydrodynamics of continuous-phase flow.[1–4]

To minimize operating costs, spray-drying systems need to be optimized in terms of energy consumption and physical properties of the product. The use of computer simulations for process optimization reduces the costs associated with experiments on real objects, for which it is necessary to, for example, stop operation of the tower. Optimization of the process based on computer simulations requires a detailed description of the parameters of heat and mass transfer between the phases, which can be determined only experimentally. Owing to simple construction and easy process control, in industrial plants, co-current systems are most common. Spray-drying systems are described extensively in the literature in terms of flow hydrodynamics,[5,6] drying kinetics,[7,8] or changes in particle morphology.[9,10]

To create effective and accurate computational fluid dynamics (CFD) models, it is necessary to understand the complex influence of process parameters and dryer geometry on the spray-drying process.[11–13] In the research units of several companies, CFD simulations are used to upgrade the design of spray dryers and to solve technological problems but details of such research are kept disclosed. However, respective models probably describe specific phenomena, not the entire process. According to Kemp and Oakley,[14] CFD modeling of spray drying is more difficult than the modeling of other methods of drying due to:

- lack of similarity in the drying dynamics during process scaling,
- strong air recirculation in the dryers that can move particles on trajectories different than air flowlines,
- dependency of morphology and quality of the product on the so-called “heating history” of the particles, and
- difficulty in determining drying kinetics for materials undergoing spray drying.

CONATCT M. Jaskulski maciej.jaskulski@p.lodz.pl Faculty of Process and Environmental Engineering, Lodz University of Technology, Wolczanska 213 Str., 90-924 Lodz, Poland.
Color versions of one or more of the figures in this article can be found online at www.tandfonline.com/ldrt.

Because of the above problems in developing the CFD spray-drying model and in gathering of experimental data, only few fully validated CFD models can be found in the literature. Most of the publications contain only theoretical descriptions without comparison with measured data.

Analysis of the literature shows that three semi-empirical models have mainly been used for the simulation of spray drying: the characteristic drying curve (CDC) model,[15,16] shortcut calculation,[17] and the reaction engineering approach (REA).[8,18,19] In the CDC approach, the drying kinetics is considered by two main drying stages. In the first drying stage, the evaporation process is calculated as for a pure solvent droplet. During the second period, which is called falling drying rate stage, drying rate is a function of the particle moisture content.[20] There are two versions of CDC that can be found in the literature: in the first one, the falling rate period can be calculated by a linear function of the particle moisture content.[16] In the second version of the CDC model, the second stage can be described with a more complex function of particle moisture content.[15] The shortcut calculation is similar to the CDC; however, the drying process is separated into three stages: constant water activity stage, penetration period, and regular regime. In the first period, drying is predicted as pure water droplet drying, whereas the other two periods are estimated experimentally. The REA uses a zero-order reaction law to describe the relation between particle surface partial pressure and mean particle moisture content.[15,21] These models (CDC, shortcut method, REA) are simple enough to calculate the interaction between the discrete phase and the gas phase, and to integrate into CFD solvers. The most advanced mathematical model of moisture evaporation based on spatial calculation of temperature and moisture gradients inside the particles implemented into the CFD was presented by Mezhericher et al.[22] However, the results of simulations performed by Mezhericher and colleagues have not been experimentally validated.

A spatially resolving model has been developed for single droplet drying (SDD)[23] at moderate and elevated temperature on the basis of SDD experiments[24] and full SDD model form.[25] Model parameters that can be used for skimmed milk and milk constituents were identified in a wide range of drying air temperatures. Additionally, inflation/deflation phenomena at high temperatures were observed and also implemented into the new SDD model. The respective methodology was described in a previous publication.[23] However, this complete SDD model is too expensive to use for spray-drying simulation by CFD. Therefore, the complete SDD needs to first be reduced to a simpler and more tractable expression of drying kinetics. For this purpose, it was decided to use the CDC approach as a reduced SDD model in the CFD environment. After validation of the developed CDC model by comparisons with results from the full SDD model and experiments, this is applied to simulate a co-current spray tower.

Particle-drying model

As discussed above, the full SDD model is too expensive to integrate into CFD. A simple model reduction will be first developed. The CDC approach is chosen as the reduced SDD model.

Mass transfer

In the CDC model, it is assumed that the relative drying rate (drying rate retardation coefficient) depends on the mean particle water content. The relative drying rate is defined as:

$$f = \frac{\dot{M}_{\mathrm{w}}}{\dot{M}_{\mathrm{w,I}}} \tag{1}$$

where $\dot{M}_{\mathrm{w}}$ is the drying rate and $\dot{M}_{\mathrm{w,I}}$ is the drying rate in the first drying stage. In the first drying stage, the relative drying rate is equal to unity. After the critical point, due to increase in internal mass transfer resistance in the particle, f decreases until it reaches $f = 0$ at the equilibrium point. Thus, evaporation rate can be defined as:

$$\dot{M}_{\mathrm{w}} = f \cdot A_{\mathrm{p}} \rho_{\mathrm{g}} \beta_{\mathrm{p}} \left(Y_{\mathrm{sr}} - Y_{\mathrm{g}} \right) \tag{2}$$

In the second drying stage f is a function of normalized particle water content, ϕ:

$$\phi = \frac{\bar{X} - \bar{X}_{\mathrm{eq}}}{\bar{X}_{\mathrm{cr}} - \bar{X}_{\mathrm{eq}}} \tag{3}$$

in which average equilibrium moisture content $\overline{X}_{\mathrm{eq}}$ can be calculated from the Guggenheim–Anderson–de Boer model:

$$\overline{X}_{\mathrm{eq}} = \frac{X_{\mathrm{mo}} c k a_{\mathrm{w}}}{(1 - k a_{\mathrm{w}})[1 - k a_{\mathrm{w}} + c k a_{\mathrm{w}}]} \tag{4}$$

Here, a_{w} is water activity (represented by relative air humidity), X_{mo} is monolayer moisture content, and c and k are parameters that depend on particle temperature:

$$c = c_0 \exp\left(\frac{\Delta H_1}{R T_{\mathrm{p}}} \right) \tag{5}$$

$$k = k_0 \exp\left(\frac{\Delta H_2}{R T_p}\right) \quad (6)$$

For skim milk subjected to drying (desorption)[26] the constants for those equations are $X_{mo} = 0.06156$, $\Delta H_1 = 24.831$ J/mol, $c_0 = 0.001645$, $\Delta H_2 = -5{,}118$ J/mol, and $k_0 = 5.710$.

Consequently, two parameters of the CDC model need to be determined: $\bar{X}_{cr}$, the average critical moisture content, and f, the function for relative drying rate prediction.

Heat transfer

Heat transfer between particle (considered uniform) and surrounding air takes place because of convection and moisture evaporation:

$$\frac{dT_p}{dt} = \frac{\alpha_p A_p (T_g - T_p) - \dot{M}_w \Delta h_{v,0}}{m_p c_p} \quad (7)$$

Mass and heat transfer coefficients were calculated from equations based on modified approach proposed by Möser[27]:

$$\alpha_p = \frac{\lambda_g}{d_p}\left(1.15\sqrt{Nu^2 + 1}\right) \quad (8)$$

$$\beta_p = \frac{D_v}{d_p}\left(1.15\sqrt{Sh^2 + 1}\right) \quad (9)$$

where thermal conductivity coefficient $\lambda_g = 0.0242$ W/mK and water vapor–air diffusivity $D_v = 2.88 \times 10^{-5}$ m^2/s.[28]

Sherwood (Sh) and Nusselt (Nu) numbers were calculated from:

$$Nu = 2 + 0.664 Re^{0.5} Pr^{\frac{1}{3}} \quad (10)$$

$$Sh = 2 + 0.664 Re^{0.5} Sc^{\frac{1}{3}} \quad (11)$$

Particle morphology changes—inflation/deflation model

The diameter of particles changes in the first drying stage because of evaporation of liquid. In the second drying stage, particle diameter can behave in two ways: if the particle temperature is lower than the boiling temperature of the solvent at the locking point, defined by the formation of a crust at the droplet surface, then the particle diameter becomes constant and equal to its critical value ($d_p = d_{cr}$).[29] However, if the temperature of the particle is higher or equal to the boiling temperature at the locking point, the particle diameter changes because of boiling of the water core.[24] After bubbling the particle diameter can increase (inflation) or the particle can be reorganized (collapse) into a smaller diameter (deflation). Those changes can be described by the following relationship:

$$d_p = d_{cr}\left(1 + K_1 \cdot \mathrm{erf}\left(\tau_{lp}\frac{t - t_{cr}}{t_{cr}}\right)\right) \quad (12)$$

where t is running time, t_{cr} and d_{cr} are the critical time and particle diameter at the locking point.

The parameter K_1 determines the final particle diameter. If K_1 is positive, this means that during the inflation/deflation period the particle grows. On the other hand, if K_1 is negative, this means that after inflation/deflation the particle collapses or shrinks and the final particle diameter is smaller than the diameter at the locking point. The parameter τ_{lp} determines the duration of the bubbling process after the locking point. Parameters K_1 and τ_{lp} were identified from SDD experiments on relatively large droplets of skim milk and approximated with the empirical equations[23]:

$$K_1 = 12.5 \cdot x_{s,0}^2 - 10.85 \cdot x_{s,0} + 2.66 \quad (13)$$

$$\tau_{lp} = -1.925 \cdot x_{s,0}^2 + 1.3945 \cdot x_{s,0} - 0.214 \quad (14)$$

where $x_{s,0}$ is the initial mass fraction of solute in the droplet.

The length of the inflation/deflation period is, however, connected to overall drying time. For this reason the τ_{lp} parameter determined during SDD experiments needs to be resized for much smaller droplets, which are more common in spray drying where drying time is much shorter. For the spray-drying simulations (with droplet diameters in the range 10–150 μm), it was assumed that the length of the boiling period can be scaled down according to the following equation:

$$\tau_{lp,r} = 0.5 + \left(\tau_{lp}\frac{d_r}{d_{p,0}}\right) \quad (15)$$

where τ_{lp} and $\tau_{lp,r}$ are dimensionless, $d_{p,0}$ in mm, and $d_r = 1$ mm.

Due to co-current flow and no recirculation of air, particle agglomeration was neglected.

Determination of CDC model parameters

The fully developed SDD model was based on drying experiments performed for skim milk droplets with diameters in the range 0.5–1.5 mm, which are much bigger than droplets used in spray drying. Additionally, air velocities used in SDD experiments are much smaller than the relative velocities between droplets and air that can appear in the atomization region, where droplets

have the initial acceleration given by the nozzle. Because SDD experiments for droplet diameters in the range 10–150 µm are difficult to perform, it was decided to scale down by using the complete SDD model for small droplet diameters. The influence of changes in droplet diameter on the evaporation process (heat and mass transfer coefficients, evaporation surface, crust formation, and inflation/deflation period) was taken into account in the complete spatially resolved SDD model.[23]

The steps involved in the reduction procedure of the CDC model (presented in Fig. 1) are as follows:

- running the complete SDD model in a sufficiently broad range of operating conditions that correspond to the conditions inside the spray tower (Table 1);
- determining the critical point (end of the first drying stage) from the full SDD model and correlating the critical water content as a function of operating parameters; and
- calculating and fitting the relative evaporation rate as a function of normalized water content.

According to this scheme, the unknown parameters of the CDC model ($\bar{X}_{cr}$ and f) are determined by fitting to drying curves calculated by the complete SDD model. Such reduction needs to be conducted within a window of operating conditions, which can appear inside the spray-drying chamber. In this frame five parameters were considered: initial solute mass fraction, inlet temperature of drying air, air velocity, inlet air moisture content, and initial droplet diameter. Respective ranges of variation used in SDD simulations are shown in Table 1. Initial droplet diameter was set in a wide range from average diameter of droplets generated by the two-fluid nozzle used in spray tower experiments to droplet diameters investigated in SDD experiments.

Locking point (critical point) is defined in the complete SDD model by local critical water content at the particle surface.[30] Average critical moisture content, $\overline{X}_{cr}$, which is also obtained from the SDD model, is the mean moisture content of the particle at the time corresponding to the locking point. After computation, respective values are correlated with the five operating condition variables. It was observed that the impact of inlet air moisture content and initial droplet diameter on the locking point can be neglected. The average critical moisture content can be calculated by ($R^2 = 0.93$):

$$\bar{X}_{\mathrm{cr}} = a_1 + \frac{b_1}{x_{\mathrm{s},0}} + c_1 T_{\mathrm{g}} - d_1 v_{\mathrm{g}}^2 + e_1 v_{\mathrm{g}} \qquad (16)$$

with $a_1 = 0.04345$, $b_1 = 0.24604$, $c_1 = 3.7652 \times 10^{-5}$, $d_1 = -5 \times 10^{-4}$, and $e_1 = 0.0045$ (T_{g} in°C, v_{g} in m/s).

The relative drying rate, f, was determined as the ratio of drying rate in the second drying period, obtained by running the full SDD model, and the drying rate at the locking point. This is exemplarily illustrated in Fig. 2. For each simulation run, an interpolation algorithm was used to get the drying rate corresponding to the same particle water content in each case.

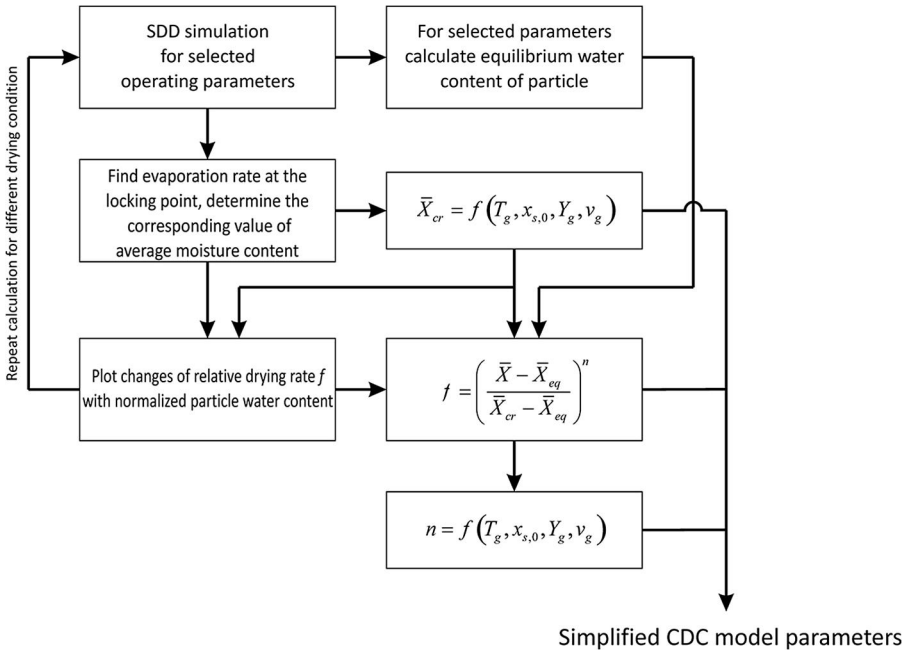

Figure 1. Scheme of the procedure used for model reduction.

Table 1. Operating conditions used in SDD model reduction.

Parameter	Range
Initial solute mass fraction, $x_{s,o}$	0.2–0.4
Inlet air temperature, T_g	60–150°C
Air velocity, v_g	0.02–15 m/s
Inlet air moisture content, Y_g	2–16 g/kg
Initial droplet diameter, $d_{p,0}$	50–2,000 µm

SDD, single droplet drying.

According to Woo et al.,[31] the retardation coefficient f may be calculated by the following equation:

$$f = \phi^n \tag{17}$$

However, it was obtained that the shape of the drying curve in the second drying stage depends on drying conditions (Fig. 3). Thus, it is proposed to extend Eq. (17) into a more complex function where the constant n is replaced by a linear function of normalized particle water content. In this case f is expressed as:

$$f = \phi^{a\cdot\phi+b} \tag{18}$$

Analysis of the simulation results shows that at low drying air temperatures ($T_g \leq 100$°C) the biggest influence on the drying process is exerted by the initial mass fraction of solute in the droplet and relative velocity of surrounding air. For the processes performed at temperatures above 100°C, it was observed that only the velocity of air affects significantly the retardation of evaporation in the second drying stage. The correlations developed for the coefficients a and b in case of low temperature ($T_g \leq 100$°C) are presented in Eq. (19) ($R^2 = 0.91$) and Eq. (20) ($R^2 = 0.98$), with v_g in m/s:

$$a = a_2 + b_2 x_{s,0} + c_2 x_{s,0}^2 + d_2 v_g + e_2 v_g^2 + f_2 v_g^3 \tag{19}$$

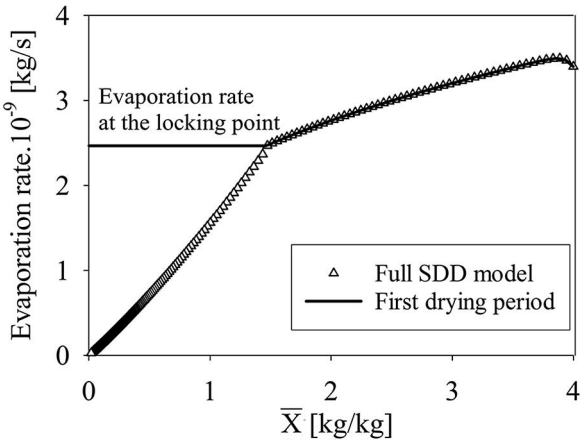

Figure 2. Illustration of the derivation of relative drying rate by comparison of the drying rate calculated from the full SDD model and the drying rate at the critical point (skim milk, $x_{s,0} = 0.2$, $T_g = 60$°C, $v_g = 0.02$ m/s, $Y_g = 4$ g/kg, $d_{l,0} = 1$ mm).

$$b = a_3 + b_3 x_{s,0} + c_3 x_{s,0}^2 + d_3 v_g + e_3 v_g^2 + f_3 v_g^3 \tag{20}$$

The factors of these equations are listed in Tables 2 and 3.

At high temperature of drying air ($T_g > 100$°C), parameters a and b can be calculated from the equations (with v_g in m/s):

$$a = 0.2465 v_g^{0.2548} \quad (R^2 = 0.93) \tag{21}$$

$$b = 0.8228 v_g^{0.0074} \quad (R^2 = 0.94) \tag{22}$$

High relative air velocities around particles in co-current flow can be only observed when the particles have the initial acceleration given by the nozzle in the atomization region. In the main part of the drying chamber, relative velocity between air and particles is very small. For those small velocities and air temperatures above 100°C, the retardation coefficient is an almost linear function of normalized particle water content φ, which confirms observations and conclusions given by Langrish and Kockel.[16]

Comparison of reduced and full SDD model

To assess the accuracy of the developed CDCs, simulation results from the reduced model (CDC) are compared with results from the full SDD model and experimental data. Exemplary comparisons at different drying temperatures are shown in Figs. 4 and 5. At the same drying conditions, the agreement between results calculated from the two models and experiments is good for both, the first and the second drying periods. In the first drying stage, the evaporation rate decreases gradually because of droplet shrinkage. The evaporation rate in the second drying stage decreases more rapidly, which is an effect of increasing internal resistances to heat and mass transfer inside the growing solid crust.

The reduced CDC model was used for calculations of spray-drying process performed by CFD simulation. The model was implemented into the ANSYS Fluent v13 solver as a user-defined function.

Experiments

Single droplet drying experiments cannot reflect fully drying conditions inside industrial spray-drying chambers. Changes in particle position cause changing conditions of the drying process, like air temperature and humidity. Additionally, local particle velocity is changing, which can have a significant influence on heat and mass transfer coefficients between discrete and continuous phase. For this reason, to perform more realistic experiments of milk spray drying, it was decided to

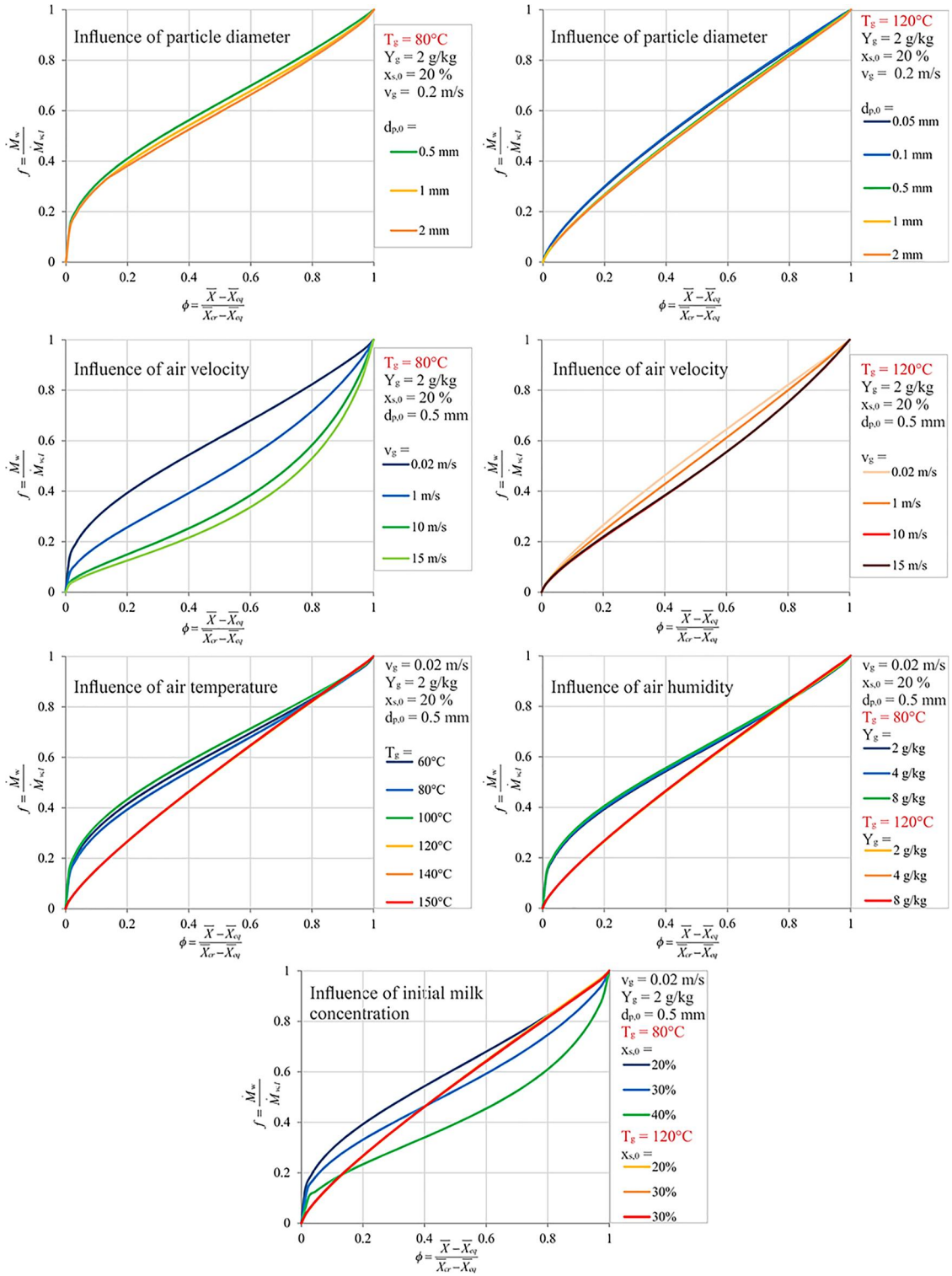

Figure 3. Influence of different drying parameters on the relative drying rate.

Table 2. Factors in equation for prediction of *a* coefficient.

a_2	b_2	c_2	d_2	e_2	f_2
−1.446	10.856	−9.895	0.569	−0.080	0.0031

Table 3. Factors in equation for prediction of *b* coefficient.

a_3	b_3	c_3	d_3	e_3	f_3
0.60	−0.92	1.807	0.112	−0.014	0.00051

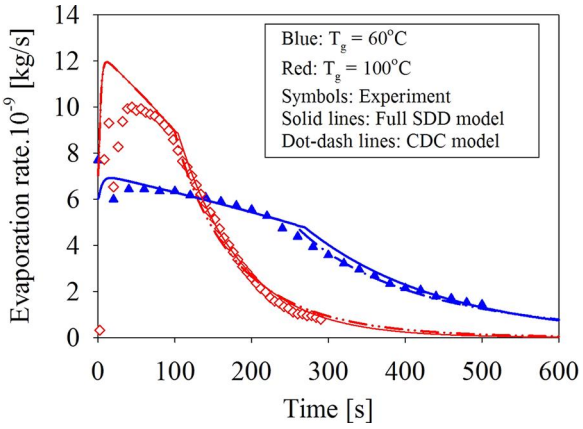

Figure 4. Comparison of evaporation rates calculated by full SDD and CDC models at low temperature $x_{s,0} = 0.2$, $v_g = 0.02$ m/s, $Y_g = 4$ g/kg, $d_{p,0} = 1.7$ mm (at 60°C), and $d_{p,0} = 1.563$ mm (at 100°C).

construct a semi-industrial, co-current spray-drying tower in the laboratory (Fig. 6).

Cold air from the laboratory hall is sucked by a fan and directed to electrical heaters. The amount of air is controlled by a computer system and can be changed by manipulation of frequency in the fan inverter. Hot air flows into the drying chamber on top of the tower. Exhausted air is separated from the dust in a cyclone and removed outside the laboratory hall.

Solution of skimmed milk (J.M. Gabler-Saliter, Germany), with initially 30% mass fraction of solid, is atomized on the top of the tower by thermostated two-fluid nozzle (model 970/0 S4, Schlick, Germany) with narrow spray angle (15–20°). Dried material is received at the bottom of the drying chamber. The total height of the drying chamber is 6.1 m with 0.4 m inner

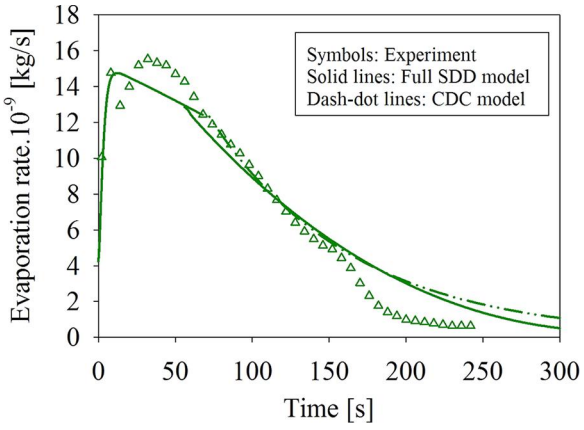

Figure 5. Comparison of evaporation rates calculated by full SDD and CDC models at high temperature ($x_{s,0} = 0.2$, $v_g = 0.02$ m/s, $Y_g = 4$ g/kg, $d_{p,0} = 1.62$ mm, $T_g = 140$°C).

diameter. Except a length of 0.72 m from the bottom, the tower is covered by 100 mm wool glass insulation.

To perform measurements of particle moisture content, four sets of measurement windows were constructed along the tower height. In each set there are two windows prepared for powder sampling (overall eight measurement levels).

Powder was caught by a metal container (350×70 mm^2) that was inserted into the drying chamber at different heights of the tower. To decrease the possibility of sample overheating and measurement mistake, powder was gathered for only 30 s. After this time the container cover was closed to protect the sample from being blown away from the container. Two samples of powder with a mass of 3–5 g each were gathered at each tower level. The first sample was used to analyze the moisture content of the powder. This analysis was performed by MA100C analyzer (Sartorius, Germany). The sample from the container was removed by a brush and immediately transported to the laboratory for the moisture analysis. Before being used again for the next measurement in the tower, the sampling container was cooled down by pressurized air. Additionally, the pressurized air was also used to remove the powder still remaining in the container. This is the second sample that was analyzed by the CamSizer XT (Retsch, Germany) to validate the particle size distribution model. The first sample is gathered by the brush to avoid additional drying, and the second with pressurized air to avoid any direct mechanical action on the powder, which might induce mistakes in particle size distribution determination. Experiments were performed for constant drying air parameters (270 kg/h, $T_{g,in} = 150$°C) and for three skim milk solution feed rates: 130, 172, and 216 mL/min (pressure of the atomization air was constant in all cases and equal to 3 bar).

Analysis of changes in air temperature inside the drying tower during operation without liquid atomization showed relatively high temperature drop (~20°C) because of heat losses to the environment. Those heat losses cannot be omitted in the CFD simulations. From calculations of changes in the air enthalpy it was found that overall heat loss was equal to 1.53 kW. To calculate the heat stream from the interior of the drying chamber to the ambient, a heat transfer model based on the mechanisms of conduction and free convection was implemented. As a result of the heat loss simulation the air temperature distribution inside the dryer was obtained and verified by comparisons with measurement data. The mean value of the heat transfer

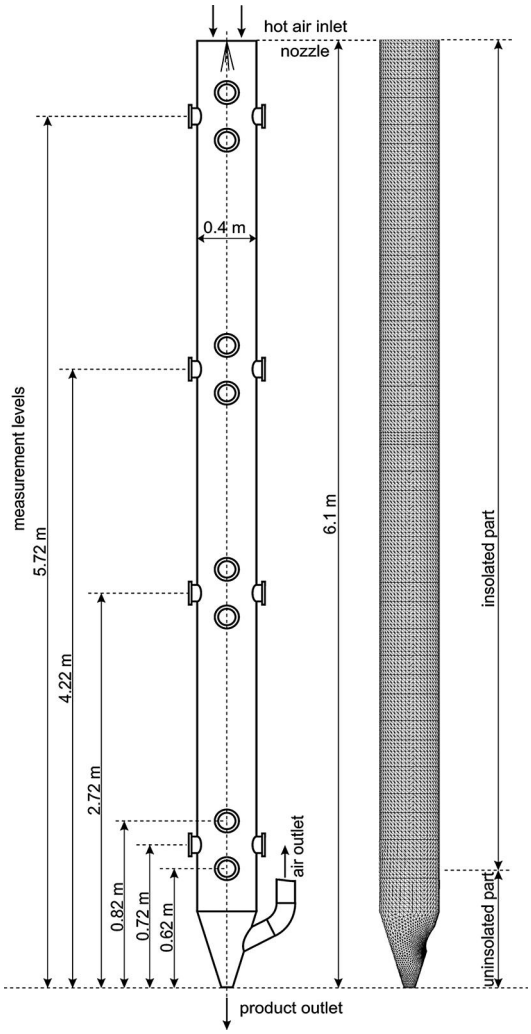

Figure 6. Schematic diagram of the experimental spray-drying tower and generated computational mesh used in CFD simulation (285,000 tetrahedral elements).

coefficient from the dryer to the ambient air was for the insulated part 4.3 W/m^2 K, while for the uninsulated part it was 7.1 W/m^2 K. Average air temperature decrease along the column was about 20°C.

CFD simulation setup

In the next step of elaborating a 3D CFD model for the co-current spray-drying process, the geometry of the tower built was simplified to reduce the number of elements of the computational mesh generated in the discretization process. Several meshes of different mesh density and element shape were tested to obtain accurate, grid-independent solution. Additionally, in the near-wall area where the highest gradients of velocity and temperature are predicted, a five-step boundary layer was generated. Finally, a mesh with 285,000 tetrahedral elements with maximum skewness of 0.79 was used in the further simulations (Fig. 6).

In the calculations three types of boundary conditions were applied: A wall-type condition was imposed on the column sides and bottom outlet. Velocity vectors in all directions are equal to zero, heat losses to the atmosphere are calculated from the heat transfer equation, and particles bounce off the walls. In the case of the wall condition imposed on the bottom particle outlet, the boundary condition for particles was set to escape. A mass flow inlet type condition was imposed on the air inlet. The condition defines air mass flow rate, temperature, and direction of air flow. An outflow pressure-type condition imposed on the bottom air outlet from the dryer allows the exhausted air to flow freely to the atmosphere. For the particles the bottom air outlet was opened.

With the experiments having a very narrow angle of spray, wall deposition observed in the cylindrical part of the drying chamber was very small. Powder was gathered only in the bottom conical part. For this reason,

Table 4. Nozzle operation and initial PSD parameters.

Feed rate (mL/min)	Atomizing pressure (bar)	Mean diameter (μm)	Spread parameter (—)	Diameter range (μm)
130	3	55	3.052	7–255
172	3	80	2.670	3–225
216	3	120	3.210	3–210

it is assumed that particles can bounce from the dryer wall. Additionally, during powder analysis we observed hardly any agglomerates in the powder produced by our spray dryer. In co-current spray drying, particles fall freely, without any recirculation into the atomization area, which is common in counter-current spray dryers. Thus, particle agglomeration and droplet coalescence were not taken into account during the simulation.

Calculations were performed in the steady-state condition with standard $k - \varepsilon$ turbulence model. Initial particle (droplet) size distribution was described by the Rosin–Rammler function, where mean particle diameter and spread parameter were determined on the base of shadowgraphy analysis (Table 4). Initial temperature of milk solution was equal to 20°C. Computation time

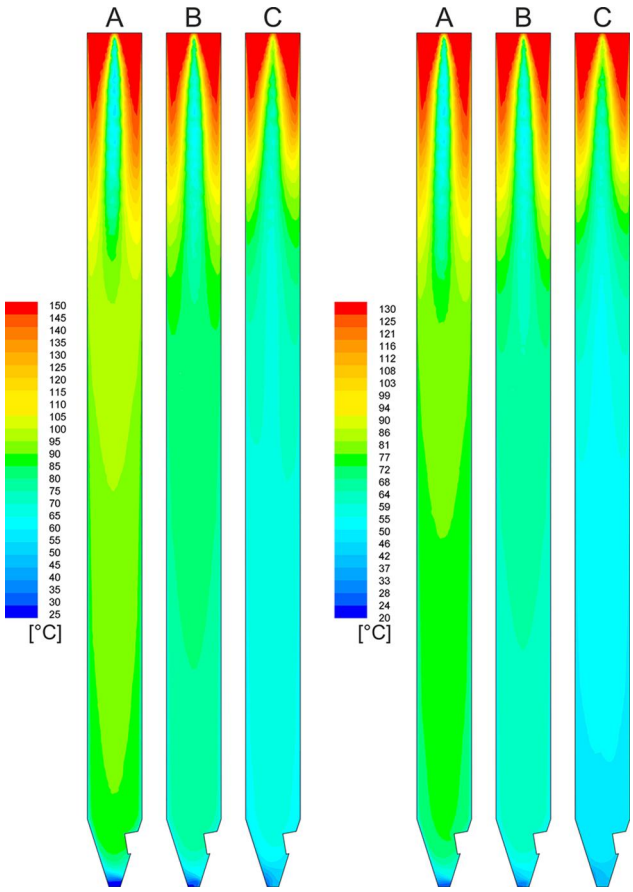

Figure 7. Profiles of moisture evaporation rate in logarithmic scale for two inlet air temperatures: 150°C (left) and 130°C (right) and for different feed rates: A—130 mL/min, B—172 mL/min, C—216 mL/min.

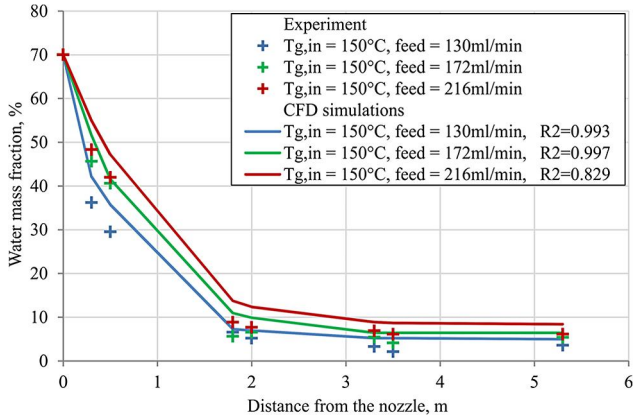

Figure 8. Changes in particle moisture content along the dryer height for different feed rates, $T_{g,in} = 150°C$.

on a simulation PC with Intel Core i7-4790 processor and 16GB RAM memory was about 1 h.

Validation of the CFD spray-drying model

To validate the developed drying model of skimmed milk in the co-current spray-drying tower, CFD simulations were made under different atomization conditions. Figure 7 shows profiles of moisture evaporation rate from the particles to the drying air presented in logarithmic scale for three different feed rates.

The spray envelope increases with increased mass flow rate of feed and decreased inlet temperature of drying air. To verify the drying model, the changes in material water content at different heights of the dryer, as obtained from the CFD simulations, were compared with experimental values. The comparison, displayed in Figs. 8 and 9 for different spray parameters, shows good agreement with the experimental data.

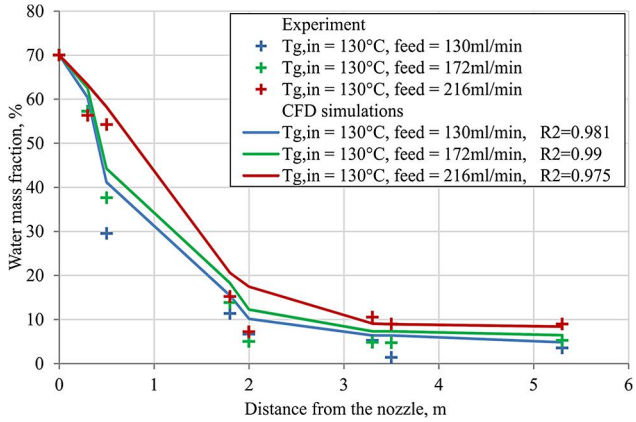

Figure 9. Changes in particle moisture content along the dryer height for different feed rates, $T_{g,in} = 130°C$.

The results of the simulation show that the process of moisture evaporation is completed at a distance of up to 4 m below the atomizing nozzle. The final moisture content of the powder depends on the feed rate, and ranges from 52.2 to 91.5 g/kg. It can be also observed that CFD simulation results are slightly higher than the values obtained from experiments. This might be attributed to the difficulty of measuring the moisture content of powder during the spray-drying process inside the drying chamber.

To perform a good measurement of the moisture content the sample needs at least to have 3–5 g of powder. Average residence time of particles inside the drying chamber ranges from 4 to 7 s. Collecting particles by the inserted container notably increases the drying time. However, the comparison shows good agreement and an appropriate response of the model to changing drying conditions.

Figure 10 shows changes in air temperature inside the drying tower for different atomization rates and initial temperatures of drying air. The temperature pattern in the drying chamber shows a symmetrical temperature distribution. Two characteristic zones of changes in air temperature profiles inside the tower can be distinguished.

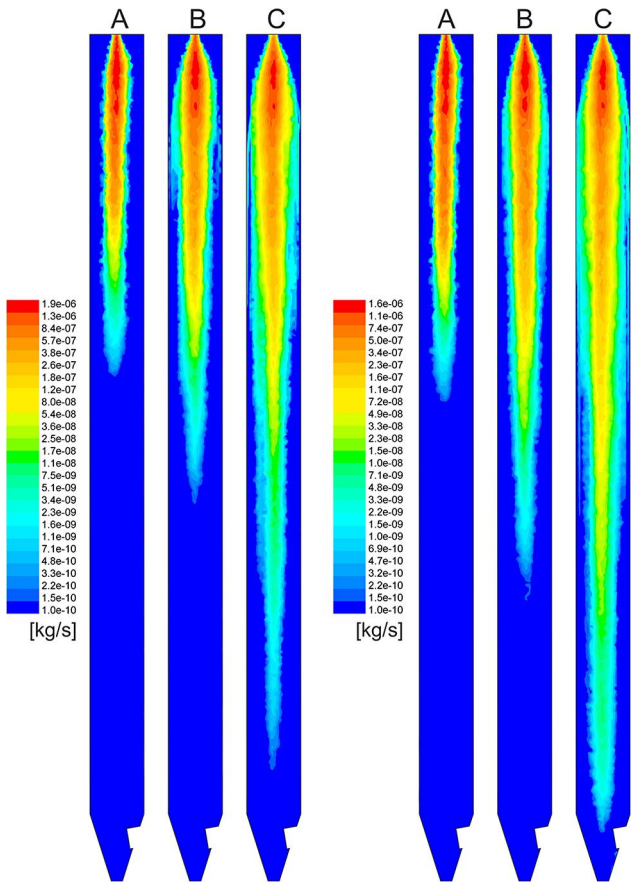

Figure 10. Air temperature profiles in axial cross-section of the dryer for two inlet air temperatures: 150°C (left) and 130°C (right) and for different feed rates: A—130 mL/min, B—172 mL/min, C—216 mL/min.

Table 5. Comparison of air temperatures at the bottom of the drying tower.

Feed rate (mL/min)	Inlet air temperature (°C)	Measured air temperature (°C)	Air temperature from CFD (°C)
130	150	96	94
172	150	87	81
216	150	79	72
130	130	77	74
172	130	67	63
216	130	60	52

The first zone of air temperature changes can be observed in the atomization region at the top of the column, where intensive moisture evaporation takes place. In the drying tower axis, where evaporation is most intense, we can observe a rapid air temperature drop. The air moving close to the chamber wall beside the spray envelope has higher temperature. The profile of air temperature changes inside the atomization zone overlaps with the evaporation rate changes presented in Fig. 7.

The second zone begins around 2 m below the nozzle; as a result of heat losses to the environment the temperature in the dryer axis is higher than the temperature near the dryer wall.

To verify the correctness of heat transfer calculations, air temperature at the level 0.85 m from the bottom of the tower was measured by a thermocouple. Because of small fluctuations of the air temperature, for the comparison time-averaged values were used. Results of the comparison are presented in Table 5.

Validation of the CFD particle morphology model

Change in the particle size during spray drying is a complex phenomenon. On the one hand, particles shrink because of moisture evaporation. On the other hand, at high temperatures, liquid can boil in the particles increasing their final diameter, or inflated particles can collapse and create small, deformed particles. Additionally, due to air recirculation, powder agglomerates can be created as a result of interparticle collisions, or due to breakage on the dryer wall small dusty fractions can appear. In co-current systems airflow recirculation is small and particle agglomeration can be neglected. However, during SDD experiments a strong influence of the drying air temperature on particle morphology has been observed. For this reason a model of particle inflation/deflation (I/D) has been developed and implemented into the CFD solver. To validate the

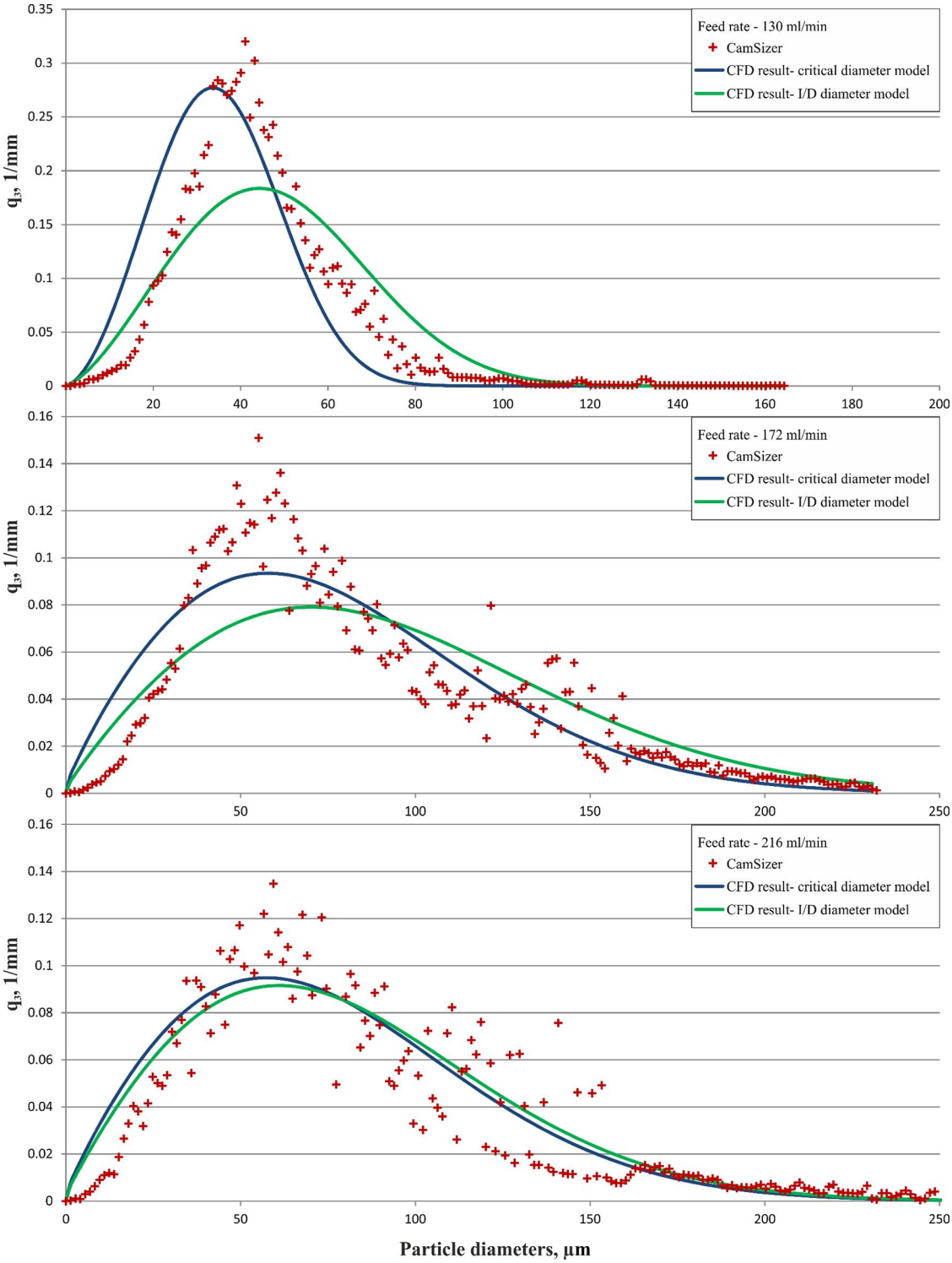

Figure 11. Comparison of particle size distributions obtained from experimental analysis and CFD simulations, $T_{g,in} = 150°C$.

I/D model, samples collected during spray-drying experiments were analyzed by the CamSizer XT and compared with the results obtained from the CFD simulations. Results of comparisons are presented in Fig. 11.

Two models of changes in particle droplet diameter were considered. The first model was the standard approach, in which particle diameter remains constant when the particle reaches the locking point. Results of this model are represented as blue lines on the following graphs. The second model was the full inflation/deflation model introduced in previous publication[23] and described previously. Results of the I/D model are presented as green lines. It can be observed that the

difference between the models decreases with increasing mass flow rate of slurry. One of the conditions of the I/D model is that at the particle locking point the temperature of surrounding air needs to be higher or equal to 100°C. By increasing the feed rate the air temperature inside of the drying chamber decreases, which leads to situations that do not fulfill the temperature condition of the I/D model; then, both models give similar results. In case with high temperature inside of the drying chamber it can be seen that the measured particle size distribution (PSD) is between the simplified critical diameter model and the full I/D calculation. However, the difference between measured values and I/D model is small and allows to implement the I/D model into the CFD solver in order to determine the PSD of the produced powder.

Conclusion

A novel methodology of determination of the CDC model parameters has been presented. The parameters of the CDC model were not determined directly from SDD experiments, but from an own, previously validated full SDD model in a broad range of operating conditions ($x_{s,0} = 0.2$–0.4, $T_g = 60$–150°C, $v_g = 0.02$–15 m/s, $Y_g = 2$–16 g/kg, $d_{p,0} = 50$–$2{,}000$ µm), which are similar to those occurring in the spray dryer. CDC model parameters, that is, the critical water content and the relative evaporation rate, were correlated as functions of the operating parameters after running the full SDD model in the above range of operating conditions. This procedure was performed to take into account changes in drying conditions inside the drying tower.

To check the correctness of the model results from the developed CDC model, results from the spatially resolving full SDD model, and SDD experiment results were compared to each other. Satisfactory accuracy of the reduced model shows that it can be applied for the entire range of drying conditions in the spray dryer. It evidences that the average critical water content and the relative drying rate of skimmed milk are not constants, as assumed in the literature, but functions of drying conditions.

Computational fluid dynamics simulations of a co-current spray-drying process of skimmed milk were performed for three different drying conditions. To show accuracy of the developed CFD model, simulation results were compared with measurement data. Good agreement of calculated changes in particle moisture content and air temperature inside the drying chamber show good accuracy of the developed CDC drying model. Additional analysis of the particle size distribution of powder allows validating the model in regard of changes in droplet diameter with and without I/D period. This CFD model can, thus, be used to optimize the performance of industrial skim milk spray dryers.

Funding

The research leading to these results has received funding from the European Union's Seventh Framework Programme for research, technological development, and demonstration under grant agreement no. 613732 – project ENTHALPY.

Nomenclature

A	surface area (m^2)
a_w	water activity (—)
c_p	specific heat capacity (J/kg/K)
D	diffusion coefficient (m^2/s)
d	diameter (m)
f	drying rate retardation coefficient (—)
$\dot{M}$	drying rate (kg/s)
m	mass (kg)
T	temperature (°C)
t	time (s)
v	velocity (m/s)
x	mass fraction (—)
X	moisture content (dry based) (kg/kg)
Y	gas moisture content (dry based) (kg/kg)

Greek letters

α	heat transfer coefficient ($W/m^2/K$)
β	mass transfer coefficient (m/s)
λ	thermal conductivity (W/m/K)
ρ	density (kg/m^3)
ϕ	normalized particle water content (—)

Subscripts, superscripts

—	average
0	initial, reference
cr	critical
eq	equilibrium
g	gas
in	inlet
mo	monolayer
p	particle
s	solute, solid
sat	saturation
sr	particle surface
v	water vapor
w	water

References

[1] Master. K. *Spray Drying: An Introduction to Principles, Operational Practice and Application*; L.Hill: London, 1972.

[2] Jaskulski, M.; Wawrzyniak, P.; Zbiciński, I. CFD model of prticle aglomeration in sray dying. *Drying Technology* **2015**, *33*(15–16), 1971–1980. doi:10.1080/07373937.2015.1081605.

[3] Huang, L.; Kumar, K.; Mujumdar, A.S. A parametric study of the gas flow patterns and drying performance of co-current spray dryer: Results of a computational fluid dynamics study. *Drying Technology* **2003**, *21*(6), 957–978. doi:10.1081/DRT-120021850.

[4] Harvie, D.; Langrish, T.; Fletcher, D.F. A computational fluid dynamics study of a tall-form spray dryer. *Food and Bioproducts Processing* **2002**, *80*(3), 163–175. doi:10.1205/096030802760309188.

[5] Masters, K. *Spray Drying Handbook*, 5th ed.; Longman Scientific and Technical: New York, 1991.

[6] Mujumdar, A.S. *Handbook of Industrial Drying*, 3rd ed.; CRC/Taylor & Francis: Boca Raton, FL/Abingdon, 2007.

[7] Zbiciński, I.; Piątkowski, M. Spray drying tower experiments. *Drying Technology* **2004**, *22*(6), 1325–1349. doi:10.1081/DRT-120038732.

[8] Schmitz-Schug, I.; Kulozik, U.; Foerst, P. Modeling spray drying of dairy products – Impact of drying kinetics, reaction kinetics and spray drying conditions on lysine loss. *Chemical Engineering Science* **2016**, *141*, 315–329. doi:10.1016/j.ces.2015.11.008.

[9] Yang, X.; Xiao, J.; Woo, M.-W.; Chen, X.D. Three-dimensional numerical investigation of a mono-disperse droplet spray dryer three-dimensional numerical investigation of a mono-disperse droplet spray dryer. Validation aspects and multi-physics exploration. *Drying Technology* **2014**, *33*(6), 742–756. doi:10.1080/07373937.2014.990565.

[10] Kwapińska, M.; Zbiciński, I. Prediction of fnal poduct poperties ater ccurrent sray dying. *Drying Technology* **2005**, *23*(8), 1653–1665. doi:10.1081/DRT-200065075.

[11] Fletcher, D.F.; Guo, B.; Harvie, D.; Langrish, T.; Nijdam, J.J.; Williams, J. What is important in the simulation of spray dryer performance and how do current CFD models perform? *Applied Mathematical Modelling* **2006**, *30*(11), 1281–1292. doi:10.1016/j.apm.2006.03.006.

[12] Langrish, T.; Fletcher, D.F. Spray drying of food ingredients and applications of CFD in spray drying. *Chemical Engineering and Processing: Process Intensification* **2001**, *40*(4), 345–354. doi:10.1016/S0255–2701(01)00113–1.

[13] Huang, L.; Kumar, K.; Mujumdar, A.S. Use of computational fluid dynamics to evaluate alternative spray dryer chamber configurations. *Drying Technology* **2003**, *21*(3), 385–412. doi:10.1081/DRT-120018454.

[14] Kemp, I.C.; Oakley, D.E. Modelling of particulate drying in theory and practice. *Drying Technology* **2002**, *20*(9), 1699–1750. doi:10.1081/DRT-120015410.

[15] Woo, M.W.; Daud, W.R.W.; Mujumdar, A.S.; Talib, M.Z.M.; Hua, W.Z.; Tasirin, S.M. Comparative study of droplet drying models for CFD modelling. *Chemical Engineering Research and Design* **2008**, *86*(9), 1038–1048. doi:10.1016/j.cherd.2008.04.003.

[16] Langrish, T.; Kockel, T.K. The assessment of a characteristic drying curve for milk powder for use in computational fluid dynamics modelling. *Chemical Engineering Journal* **2001**, *84*(1), 69–74. doi:10.1016/S1385–8947(00)00384–3.

[17] Kieviet, F.G. Modelling quality in spray drying. Ph.D. thesis. Eindhoven University of Technology, Netherlands, 1997.

[18] Rogers, S.; Fang, Y.; Qi Lin, S.X.; Selomulya, C.; Dong Chen, X. A monodisperse spray dryer for milk powder: Modelling the formation of insoluble material. *Chemical Engineering Science* **2012**, *71*, 75–84. doi:10.1016/j.ces.2011.11.041.

[19] Gao, X.; Wang, J.; Wang, S.; Li, Z. Modeling of drying kinetics of green peas by reaction engineering approach. *Drying Technology* **2015**, *34*(4), 437–442. doi:10.1080/07373937.2015.1060491.

[20] Keey, R.B.; Suzuki, M. On the characteristic drying curve. *International Journal of Heat and Mass Transfer* **1974**, *17*(12), 1455–1464. doi:10.1016/0017–9310(74)90055–6.

[21] Chen, X.D.; Putranto, A. *Modeling Drying Processes: A Reaction Engineering Approach/by Xiao Dong Chen, Aditya Putranto*; Cambridge University Press: Cambridge, 2013.

[22] Mezhericher, M.; Levy, A.; Borde, I. Spray drying modelling based on advanced droplet drying kinetics. *Chemical Engineering and Processing: Process Intensification* **2010**, *49*(11), 1205–1213. doi:10.1016/j.cep.2010.09.002.

[23] Tran, T.T.H.; Jaskulski, M.; Avila-Acevedo, J.G.; Tsotsas, E. Model parameters for single droplet drying of skim milk and its constituents at moderate and elevated temperatures model parameters for single droplet drying of skim milk and its constituents at moderate and elevated temperature. *Drying Technology* **2017**, *35*(4), 444–464. doi:10.1080/07373937.2016.1182548.

[24] Tran, T.T.H.; Avila-Acevedo, J.G.; Tsotsas, E. Enhanced methods for experimental investigation of single droplet drying kinetics and application to lactose/water. *Drying Technology* **2016**, *34*(10), 1185–1195. doi:10.1080/07373937.2015.1100202.

[25] Mezhericher, M.; Naumann, M.; Peglow, M.; Levy, A.; Tsotsas, E.; Borde, I. Continuous species transport and population balance models for first drying stage of nano-suspension droplets. *Chemical Engineering Journal* **2012**, *210*, 120–135. doi:10.1016/j.cej.2012.08.038.

[26] Chen, X.D.; Lin, S.X.Q. Air drying of milk droplet under constant and time-dependent conditions. *AIChE Journal* **2005**, *51*(6), 1790–1799. doi:10.1002/aic.10449.

[27] Möser, C. *Die desorption von ammoniak aus wassertropfen im ultraschall-stehwellenfeld: Experiment und modellbildung*. Dissertation. Otto-von-Guericke-Universität Magdeburg, Germany, 2001.

[28] Perry, R.H.; Green, D.W. *Perry's Chemical Engineers' Handbook*, 8th ed.; McGraw-Hill Professional: London/McGraw-Hill [distributor]: New York, 2008.

[29] Tsotsas, E. Multiscale approaches to process that combine drying with particle formation. *Drying Technology* **2015**, *33*(15–16), 1859–1871. doi:10.1080/07373937.2015.1047954.

[30] Jaskulski, M.; Tran, T.; Peglow, M.; Avila-Acevedo, J.; Tsotsas, E., Eds. An advanced modelling and experimental validation of single droplet drying process. In *Proceedings of the EFFoST International Conference*; Athens, Greece, November 10, 2015.

[31] Woo, M.W.; Daud, W.R.W.; Mujumdar, A.S.; Wu, Z.; Meor Talib, M.; Tasirin, S.M. CFD evaluation of droplet drying models in a spray dryer fitted with a rotary atomizer. *Drying Technology* **2008**, *26*(10), 1180–1198. doi:10.1080/07373930802306953.